Review of Rate Constants for the Thermal Dissociation of Dinitrogen Oxide (N_2O) and the $O(^3P) + N_2O$ reaction

A.M. Ekwonu[1], C.I. Egwuatu[2] & P.U. Umennadi[3], C. M. Okey-Nzekwe[4],
Department of Pure and Industrial Chemistry
[1.4]Chukwuemeka Odumegwu Ojukwu University, Anambra State.
[2]Nnamdi Azikiwe University, Awka Anambra State
[3]Tansian University, Umunya Anambra State

Abstract. The rate of the reaction of N_2O with $O(^3P)$ was investigated experimentally and by kinetic modelling using Arhenius equations but only over a limited temperature range of $1200 \leq T \leq 1400k$ was applied. Upper limit values of the overall rate constant for the $N_2O + O(^3P)$ reaction were estimated by a statistical technique. These values obtained were about a factor of 10 lower when compared with an overall uncertainty of about a factor of three than those calculated from the recommended Arhenius expressions of previous scientist. The thermal dissociation of N_2O in argon was carried out and investigated by monitoring the formation of $O(^3P)$ atoms in the reflected shock regime using Atomic Resonance Absorption Spectro-photometry (ARAS). The total density and N_2O ranges were between $(2.6x10^{18})$- (5.4×10^{18}) molecules cm^{-3} and $(3.3 \times 10^{12}) - (7.9 \times 10^{15})$ molecules cm^{-3} respectively.The values for the bimolecular rate constant derived under low-pressure limit conditions are given by the Arhenius expression: $K(T) = (1.18 \pm 0.16) \times 10^{-9} \exp(-57820 \pm 460 \text{ cal mol}^{-1}) /RT \text{ cm}^3 \text{ molecule}^{-1} \text{ s}^{-1}$ for the temperature range of $1195 \leq T \leq 2384k$. these results extend the low-temperature range of Atomic Resonance Absorption Spectrophotometry measurements of K_1 by about 200^{oc} which is very significant in I/T; and the value of the rate constant was extended by more than an order of magnitude. Uncertainties in the Arhenius expression are given at the one standard deviation level and the mean deviation of the experimental data from that predicted by the expression is ± 26%.

Keywords: Thermal dissociation, Rate constants, N_2O, (O^3P) and N_2O Reaction. (Arrhenius equation & Beer Lambert's law applied)

1. INTRODUCTION

The thermal dissociation of N_2O is of continuing interest both in experimental and theoretical chemistry, and in technological processes such as combustion in fluidized beds, combustion under fuel lean conditions, and propellant combustion (Johnson, J. E. et, al. 1992). Consequently, there have been numerous experimental and theoretical studies to establish the kinetics and the dynamics of this reaction (Dean, A.M, 1976). In addition, the Kinetics of this system are discussed in review article by (Baulch, D.L et, al. 1973).

Studies of this unimolecular reaction shows that reaction proceeds through a spin-forbidden, non adiabatic pathway to form $o(^3P)$ atoms in preference to the spin allowed, but more endothermic dissociation to form O (ID) atoms according to the equation below:

$$N_2O\ (^1\Sigma^+) + M \rightarrow N_2\ (^1\Sigma_g^+) + O(^3P) + M$$
$$\Delta_1 H^0_0 = 39 \text{ Kcal mol}^{-1} - (1)$$
$$N_2O\ (^1\Sigma^+) + M \rightarrow N_2\ (^1\Sigma_g^+) + O(^1D) + M$$
$$\Delta_1 H^0_0 = 84 \text{ Kcal mol}^{-1} - (2)$$

Dissociation occurs as a result of collision induced vibrational excitation of the singlet ground state to a critical "energy level" from which intersystem crossing takes place to a triplet state, which is predissociative (Bauch, D.L et.al, (1973). Various analytical techniques such as mass spectroscopy, gas chromatrography, Uv-vis emission absorption and absorption spectrophotometry were employed in these investigations. There are significant differences in the bimolecular rate constant expressions found, particularly among the activation energy values, which range from about 48 to 62 kcal mol^{-1}. The non ARAS results, in particular, show the widest variability in values for the apparent activation energy and for the individual values of K(T). In contrast, results from studies that employed the ARAS technique display reasonably close agreement, especially a narrow range in activation energies with most values chestering around 61 Kcal mol^{-1}.

In theoretical study, the potential energy surfaces involved were calculated and critical information on the crossing surfaces linking the ground state singlet to the three possible triplet states were provided (Cheng and Yarkong, 1993). These authors further show that only the linear A" triplet state is important with state to state crossing occurring at an energy level of about 58 Kcal mol^{-1} above the ground state. This calculated energy level should relate to the high-pressure activation energy for reaction RI. If so, the value of 58 K cal mol -1 would appear to be somewhat small in relation to both the majority of the low-pressure. ARAS results (≈ 61 Kcal mol^{-1}) and to the recently value for the high-pressure limit (Rohrig, et al, 1996) $E_{a^{\infty}}$ = 62.6 K cal mol^{-1}.

Fall-off behaviour and the asymptotic approach to the high pressure limit is observed only at very high pressure (Mallard, W.G. et, al. 1994) clearly a precisely defined kinetic expression for the low pressure rate constant is required to test future unimolecular calculations and for modeling of combustion systems.

2. MATERIALS AND METHODS

2.1 Experimental Procedure:

The shock tube apparatus, its operation, and its subsequent modifications were done using standard procedure as described by (Klemn, R.B, et, al., 1992). The shock tube was operated in the thermal mode, ARAS which was used to monitor changes in the concentration of O-Atom photometer (i.e $O(^3P)$ atoms).

The temperature (T_5), density (P_5) and pressure (P_5) in the reflected shock regime were calculated using ideal shock theory from the measured values of the incident shock velocity, the test gas composition, the initial temperature, and the initial pressure. Vibrational equilibrium was assumed to be complete. When necessary, boundary layer effects were corrected for by a procedure that made use of the adiabatic equation of state and of the experimental measurements of the pressure changes occurring in the sample after passage of the incident and reflected shock waves. Uncertainties in determining Mach numbers ranged from 0.5 to 1% leading to corresponding uncertainties in T_5 and P_5 of 1-2%.

2.2 Application of Beer- lamberts law:

The resonance lamp was operated at a pressure of 10 Torr with a mixture of 0.0862% of 0_2 in He and a microwave power level of about 100w. An O-atom filter, which consisted of a second microwave discharge in a flowing mixture of 9.54% 0_2 in He that was maintained at 8 Torr, was located between the lamp and the shock tube window. A vacuum Uv Caf_2 window, placed in the optical path between the filter and the shock tube window, allowed transmission of the O-atom resonance triplet lines, centered at 130.4nm, but effectively blocked the lower lying resonance line emissions from H and N atoms. The photomultiplier housing was purged by a steady flow of N_2. When the voltage signal from the photomultiplier was measured with the

filter discharge on and off, the fraction of incident resonance radiation was determined. If F is the fraction of resonance radiation, lo is the total incident intensity (Vo volts) and I_t is the transmitted intensity at time t. It is assumed that the Beer-lambert law (ABS =α/c) holds, where α is the O – atom absorption coefficient (Cm^2 molecule $^{-1}$), L is the path length (the diameter o the shock tube, 6.02cm^3, and c is the O – atom concentration (molecules cm^{-3}).

The base line level $l_o = V_o$ is usually taken as the signal level in the reflected regime immediately following the passage of the shock front past the observation widow. At very high temperatures, where it can be obscured by the fast formation of atoms, the base line is determined from corresponding absorbance values associated with compression ratios measured at lower temperatures with appropriate concentrations of reactant mixtures. Where the rate constants were derived from the initial linear slope of the O-atom absorbance Vs time, the base line could be easily determined with sufficient accuracy by extrapolation.

2.3 O-atom Calibration:

The O-atom spectrophotometer was calibrated by completely dissociating N_2O at known mole fractions ($1.040 \times 10^{-6} \leq x\ N_2O \leq 9.740 \times 10^{-6}$) in argon over the temperature range of $1932 \leq T \leq 2384$k. A typical transmittance-time profile from a calibration run is shown in figure. I, the initial voltage signal rapidly decreasing with time after the passage of the reflected shock, to reach a constant level, corresponding to the final concentration of O-atoms when N_2O has fully dissociated, Experimental conditions are chosen so that secondary reactions are negligible, and therefore the final concentration of O – atoms $[O]_\infty$ is equal to the initial concentration of N_2O. A calibration plot can then be constructed that shows the relationship between absorbance and O-atom concentrations.

2.4 Molecular Absorption at High Concentrations of N_2O:

Incident radiation from resonance H and O – atom lamps contains a significant fraction from resonance H and O – atom lamps which contains a significant fraction of non-resonance light that can range from 10 to 35% depending on lamp operating conditions. The resonance light fraction f, necessary for the calculation of absorbance and atom concentration, is usually determined at ambient temperature for the evacuated shock tube as has been previously described (Michael, J. V et. al, 1986). In general, the absorption coefficients of molecular components at resonance wavelengths are very much less than those of the H and O – atoms, ranging from $10^{-18} – 10^{-20}$ cm^2 $molecule^{-1}$. These values are to be compared to absorption coefficients of 10^{-13}- $10^{-14}cm^2$ $atom^{-1}$ for Hydrogen and $10^{-14} – 10^{-15}cm^2$ $atom^{-1}$ for O – atoms observed with typical resonance lamps. Careful turning of the microwave cavity, the lamp design itself, and appropriate choice of operating conditions enable bright, stable, and reproducible plasmas that emit 75 – 90% of incident resonance light to be formed. The use of a solar blind photomultiplier further minimize the effect of absorption of non-resonance radiation by molecular components. Usually, in the typical ARAS shock tube experiment, the small perturbations in the value of the light fraction, caused by light absorption by the molecular components of the mix, are not significant and thus the light fraction is little changed in the reflected regime. Moreover, these small perturbations have even a more minor effect on the accuracy of the rate constant determination, especially when compared to the typical errors that result from the uncertainties in determining the temperature, pressure, and density in the reflected regime.

3 RESULTS AND DISCUSSION

The results of the analysis conducted above are presented here in tables below followed by their respective figures for illustrations.

Table 1: Results of Low-Pressure Rate Constant Expressions Determined by Shock Tube Techniques for $N_2O + M \rightarrow N_2 + O(^3P) + M$, M = Ar

temperature (K)	pressure (Torr)	A (cm^3 molecule s^{-1})	E. (kcal mol^{-1})
1850-2500	13,50	2.40×10^{-9}	61.206
1519-2408		2.23×10^{-9}	62.040
1450-2200	760-1350	2.40×10^{-9}	59.465
1600-2500	760	1.66×10^{-9}	60.470
1540—2500	11	2.76×10^{-10}	52.542;
Rate Expressions Determined via Other Diagnostic Techniques			
1500-2500	80-250	1.66×10^{-9}	60.999
1500-2500	1 140-2.28 x 10^5	8.32×10^{-10}	57,998
1000-2000	30-200	8.32×10^{-10}	57.001
1000-3000		7.80×10^{-10}	58. 001
1850-2536	60-74	4.90×10^{-10}	52.367
2160-2500	2-75	8.32×10^{-10}	58.000
1950-2800	37-77	1.91×10^{-10}	48.639
2100-3200	77-238	4.50×10^{-10}	54.016
1815-3365	304-380	2.36×10^{-10}	51.282
1700-2400	1 12-744	6.47×10^{-10}	57.365
1688-3113	228-4560	5.25×10^{-10}	55.834
1685-2560	1290-3500	6.15×10^{-10}	54.966
1820.-3170	186-435	7.30×10^{-10}	56.001.
Rate Expressions Recommended in Review Articles			
1300-2500		8.30×10^{-10}	57.623
1500-2500		5.61×10^{-10}	56,761
1000-2500		1.75×10^{-9}	60.521

Table 2: Results of High-Pressure Hate Constants for $N_2O + M \rightarrow N_2 + O(^3P) + M$

temperature (K)	pressure (Torr)	A, (s^{-1})	En (kcal mol^{-1})
1400-2500	(6.08×10^2)-(2.28×10^5)	1.26×10^{11}	59.5
1250-1800	(5.32×10^3)-(7.60×10^3)	9.3×10^{10} [a]	52.8
1780-2300	(1.52×10^3)-(1.55×10^4)	1.7×10^{11}	57.6
1103- 1173	(1.14×10^3)-(7.98×10^3)	5.3×10^{10} [a]	56.02
1600-2000	(2.28×10^2)-(3.42×10^5)	1.3×10^{12}	62.61

"This value has been corrected for collision efficiency: (ArJ = $[N_2]$/1

Table 3: Results of the Calibration Data for the O-Atom Photometer

P_1/Torr)	M_s[b]	P_5[c]	T_5/K[d]	ABS.	P_5 (N_2O)[c]	P_1/Torr)	M_s[b]	P_5[c]	T_5/K[d]	ABS_	P_5 (N_2O)[c]
					$X_{N2O} = 1.040 \times 10^{-6}$						
15.11	2.947	3.173	2092	0.13	3.300	15.06	2.996	3.200	2159	0.13	3.328
15,11	2.959	3,181	2110	0.13	3.308						
					$X_{N2O} = 1.058 \times 10^{-6}$						
15.07	2.971	3.200	2114	0.13	3.386	15.08	2.925	3.158	2056	0.13	3.341
15.07	2.936	3.160	2075	0.14	3.343	15.06	2.983	3.202	2132	0.14	3.3S8
15.00	2.887	3.108	2008	0.14	3.288	14.85	3.016	3.189	2173	0.13	3.374
14.89	2.96?	3.151	2106	0.14	3.334	15.06	2.957	3.185	2095	0.14	3.370
					$X_{N2O} = 1.655 \times 10^{-6}$						
15.53	2.929	3.245	2069	0.21	5.370	15.63	2.824	3.172	1932	0.20	5.250
					$X_{N2O} = 2.014 \times 10^{-6}$						
15.00	2.892	3.112	2014	0.27	6.268	14.98	3.004	3.204	2159	0.27	6.453
15.08	2.884	3.126	2000	0.26	6.296	15.03	3.019	3.228	2179	0.27	6.501

15.06	2.921	3.153	2050	0.26	6.350	15.06	2.948	3.173	2086	0.26	6.390
15.07	2.937	3.165	2072	0.25	6.374						
					$X_{N2O} = 2.322 \times 10^{-6}$						
15.06	3.025	3.224	2198	0.26	7.486	15.03.	2.860	3.083	1976	0.26	7.159
15.00	3.095	3.261	2296	0.27	7.572	15.02	3.021	3.212	2192	0.27	7.458
					$X_{N2O} = 2.404 \times 10^{-6}$						
15.06	2.897	3.125	2024	0.29	7.513	15.02	3.157	3.312	2383	0.28	8.001
14.98	3.030	3.209	2204	0.30	7.714	15.04	3.165	3.328	2391	0.28	7.963
15.05	2.864	3.087	1984	0.29	7.421	15.00	3.053	3.234	2235	0.29	7.774
10.30	3.143	2-266	2361	0.22	5.447	15.08	3.082	3.272	2276	0.30	7.866
					$X_{N2O} = 2.727 \times 10^{-6}$						
15.74	3.118	3.476	2305	0.32	9.479	14.91	2.973	3.158	2122	0.32	8.612
15.65	2.903	3.254	2029	0.32	8.874	15.64	2.998	3.324	2163	0.32	9.065
					$X_{N2O} = 3.150 \times 10^{-6}$						
14.94	2.967	3.151	2120	0.37	9.926	15.14	2.921	3.157	2059	0.37	9.945
15.15	2.924	3.160	2063	0.36	9.954						
					$X_{N2O} = 3.266 \times 10^{-6}$						
15.05	3.011	3.212	2178	0.39	10.490	14.99	3.027	3.200	2208	0.37	10.451
15.09	3.028	3.225	2206	0.36	10.533	15.02	2.87.3	3.092	1995	0.39	10.098
					$X_{N2O} = 4.120 \times 10^{-6}$.						
15.02	3.107	3.278	12311	0.48	13.505	15.23	2.947	3.198	2091	0.50	13.176
15.03	2.965	3.171	2116	0.49'	13.065	15.05	3.108	3.288	2311	0.47	13.547
					$X_{N2O} = 5.191 \times 10^{-6}$						
15.04	3.035	3.270	2182	0.59	16.974	15.06	2.879	3.107	2001	0.60	16.128
15.02	3.032	3.239	2194	0.60	16.814	15.03	2.983	3.188	2139	0.57	16.549
15.13	3.033	3.239	2213	0.58	16.184						
					$X_{N2O} = 5.807 \times 10^{-6}$						
14.98	3.034	3.220	2205	0.66	18.699	14.92	3.056	3.221	2237	0.64	18.704
15.02	3.029,	3.223	2200	0.67	18.716	15.07	2.843-	3.079	1954	0.67	17.880
					$X_{N2O} = 7.755 \times 10^{-6}$						
14.88	2.995	3.185	2142	0.86	24.700	15.02	2.914	3.153	2030	0.86	24.451
15.29	3.000	3.273	2150	0.84	25.382	13,41	3.106	3.384	2295	0.83	26.243
15.05	2.935	3.171	12063	0.86	24.591						
					$X_{N2O} = 9.740 \times 10^{-6}$						
15.33	2.995	3.287	2137	1.00	32.015	15.03	3.047	3.259	2211	0.97	31.743
15.08	2.990	3.230	2,131	1.00	31.460	15.17	2.891	3.155	2006	1.06	.30.730
					$X_{N2O} = 3.956 \times 10^{-6}$						
15.85	2.957	3.366	2087	0.49	1.332	15.76	3.091	3.451	2270	0.51	1.365
15.87	3.086	3.477	2262	0.50	1.376	15.32	3.174	3.43/3	2376	0.50	1.359
15.80	2.945	3.381	2051	0.49	1.338	15.23	3.174	3.404	2384	0.50	1.347

Table 4: Result of Absorbance Data obtained from Nonresouance Light (O-Atom Filter On)

$V^{AT}{}_{NR}{}^{a}$	$V^{1}{}_{NR}{}^{b}$	$V^{R}{}_{NR}{}^{c}$	$ABS^{1}{}_{NR}$ d	$\Delta[N_2O]^{e}$	$ABS^{R}{}_{NR}{}^{f}$	$\Delta[N_2O]^{g}$
32.83	28.02	24.07	0.1584	1.864	0.3104	5.035
35.21	30.88	27.00	0.1312	1.511	0.2655	4.035
26.00	24.78	23.57	0.0480	0.3659	0.0980	0.9801
52.36	44.97	38.80	0.1521	1.82.5	0.2997	5.174
52.38	44.77	38.45	0.1570	1.641	0.3092	4.643
54.59'	48.61	42.85	0.1160	1.079	0.2421	'3.090
55.61	50.41	45.25	0.0982	0.8663	0.2062	2.447.
56.76	50.68	44.93	0.1133	1.034	0.2337	2.763
57.19	51.29	45.64	0.1089	1.012	0.2256	2.724
58.12	53.37	48.24	0.08537	0.7159	0.1865	2.028
47.78	43.88	39.56	0.08517	0.7100	0.1889	2.010
45.91	42.81	39.10	0.06995	0.5673	0.1606	1.622

27.65	26.31	24.62	0.04968	0.3765	0.1161	1,015

Table 5: effect of changing light fraction value on rate constants

T (K)	XN_2O	Light fraction (uncorrected, f^{AT})	light fraction (corrected, f_{CORR})	percent change"
1500	2.403×10^{-4}	0.65	0.62	5.3
1378	2.403×10^{-4}	0.63	0.58	8.1
1409	4.176×10^{-4}	0.64	0.56	16.0
1425	1.000×10^{-3}	0.62	0.50	33.0
1322	2.000×10^{-3}		0.38	150.0

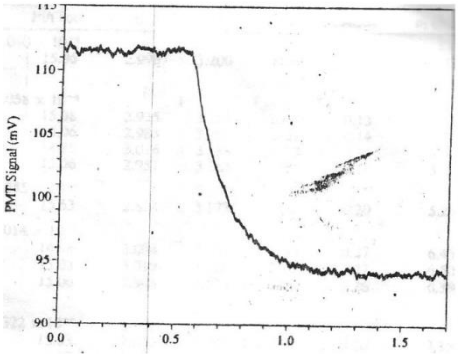

Figure 1: Typical transmission signal observed for the thermal decomposition of N_2O in the reflected shock regime.

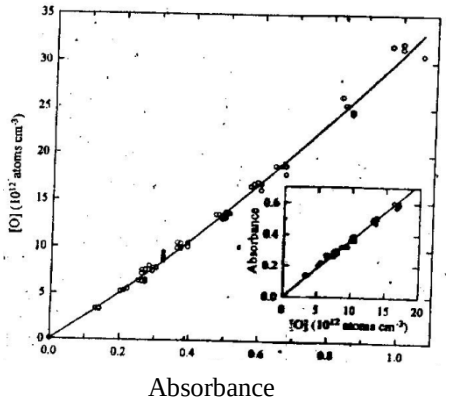

Absorbance

Figure: 2: Calibration data for the solid line fit of the polynomial of degree 2 to absorbance, data from 0 to 1. l(i.e open and filled circle data from punfied 99.99% of N_2O).

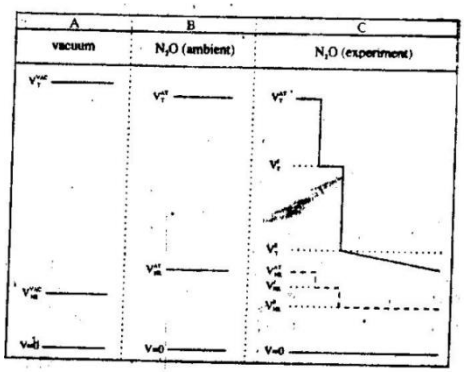

Figure 3: Schematic of transmission changes observed when a high concentration of N_2O mixture is shocked.

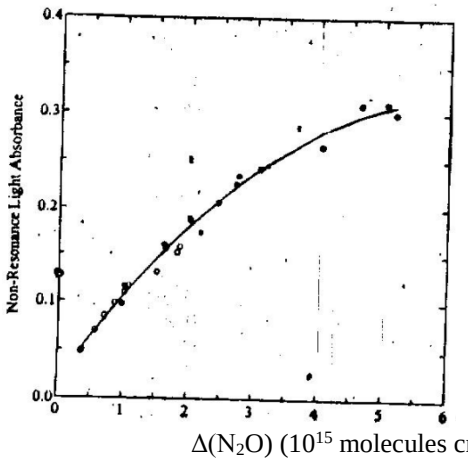

Figure 4: Calibration curve for determination of the non-resonant light absorbance by N_2O.

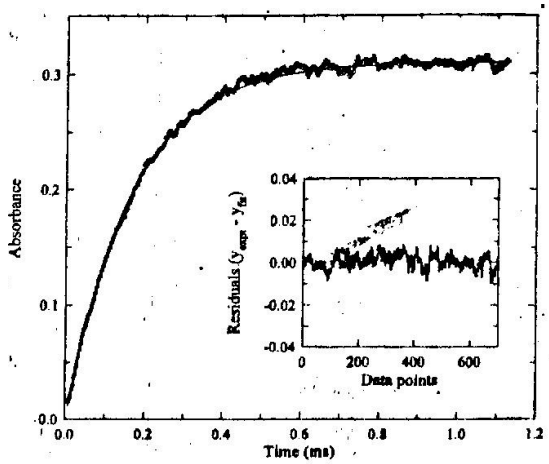

Figure 5: Plot of the absorbance build up corresponding to the transmission signal of fig. 1.

4 DISCUSSION

The expression tabulated here in table one is for M = Ar which was corrected for collision efficiency; [Ar] = [N_2]/1.5). The values for A and E_a given in table one were evaluated from the rate constant data for the experiments performed with Ar diluents. The rate expression was conducted severally and obtained by using least-squares analysis to give a linear fit over the temperature range of T = 1500-2500k, T = 1500-3600k, T = 700-2500k and T = 1000 – 2500k respectively. The values in table 2 of high-pressure Rate constants for $N_2O + M \rightarrow N_2 + O(^3P) + M$ was also corrected for collision efficiency: (Ar) = [N_2]/1.5 A full description of N_2O thermal decomposition requires that reactions in equ (3) and equ (4) be considered along with reaction in equ (1)

$O(^3P) + N_2O \rightarrow NO + NO$ – equ (2a)

$O(^3P) + N_2O \rightarrow N_2 + O_2$ – equ (2b)

At high concentrations of N_2O and where substantial decomposition takes place, the following additional reactions may also become significant:

$O(^3P) + NO + Ar \rightarrow NO_2 + Ar$ – equ (3)

$O(^3P) + N_2O \rightarrow O_2 + NO$ – equ (4)

$NO + N_2O \rightarrow NO_2 + N_2$ – equ (5)

$O(^3P) + O_2 + Ar \rightarrow O_3 + Ar$ – equ (6)

$NO + O_3 \rightarrow NO_2 + O_2$ – equ (7)

The reactions above were relatively slow, and until recently, both channels were thought to be of nearly equal importance,

$K_{2a} = 1.1 \times 10^{-1} \exp(-13400/T)$ cm^3 $molecule^{-1}$

$s^{-1} = 1.7 \times 10^{-10} \exp(-14100/T)$ cm^3

Unless otherwise stated, the N_2O sample in table 3 was of 99.99% purity. The uncertainty in measuring the Mach number is typically about ± 0.7%. at the one standard deviation level. Units of density are 10^{18} molecules cm^{-3}. The uncertainty in temperature is estimated to be no more than ± 1.5%. Units of density are 10^{12} molecules cm^{-3}. The N_2O sample for these data was of 99.99% purity.

"Initial voltage le.vel at room temperature before shock compression; units are mV. Voltage level after incident shock compression; units are mV. Voltage level after reflected shock compression;, units are mV. Nonresonance absorbance after incident shock compression; $ABS^1_{NR} = \ln(V^{AT}_{NR}/V^1_{NR})$. Change in N_2O concentration after incident shock compression; units are molecules $cm^{-3} \times 10^{15}$.[f] Nonresononce absorbance after reflected shock compression; $ABS^RNR = \ln(V^{AT}_{NR}/V^1_{NR})$. Change in N_2O concentration after reflected shock compression; units are molecules $cm^{-3} \times 10^{15}$.

Table 5 shows the percentage change in the rate constants that employed the correct light fraction.

The N_2O + M (Ar) Reactions, the rate constant for reaction in equ (1) has been demonstrated to be in the low-pressure limit for pressures ≤ 6 atm. Since the present experiments were performed at pressures below 1 atm, the data were computed as second-order rate constants.

In kinetic analysis of first order method, at high temperatures (T > 1900k) the reaction goes to completion within the experimental observation time, and the low-pressure unimolecular rate, first order in [Ar] and [N_2O], is then given by :

$-d[N_2O]/d_t = d[O]/d_t = k_1 [Ar][N_2O]_t$ equ (8)

Hence , K_1 can be determined from the slope of the first-order plot.

$In([O]_\infty - [O]_t) = - k_{abs}{}^t + In[O]_\infty$ equ (9)

Where $k_{abs} = k_1 [Ar]$.

It is assumed that the Beer-Lambert law (ABS = α/c) holds, where α is the O-atom absorption coefficient (cm^2 $molecule^{-1}$), l is the path length (the diameter of the shock tube, 6.02cm), and c is the O-atom concentration (molecules cm^{-3})

Figure 2 and 3 show the calibration data of solid line that is fit for the polynomial of degree and schematic transmission changes observed when a high concentration mixture is shocked. Fig. (4) shows the calibration curve for determination of the non resonant light absorbance by N_2O. The calibration data are listed in table (4) and shown in fig. (4).

5 CONCLUSION

Shock tube experiments were performed, with sensitive; ARAS detection of oxygen atoms, to measure the rate constant for N_2O thermal dissociation at the low-pressure limit over the temperature range of 1195 5 T ≤ 2384 K. A procedure to correct for molecular absorption of resonance and non resonance light by N_2O allowed rate constant measurements to be extended by almost 200° to just below 1200 K, which is significant in terms of 1/T. Also, by extending measurements down to 1200 K, this work provides ARAS data for reaction Rl that, for the first time, overlap with previous studies that employed non shock tube techniques.

The ARAS rate data from five independent studies in five laboratories were combined with the present data for reaction Rl and represented by the Arrhenius expression,

$K_1(T) = (9.52 \pm 1.07) \times I0^{-10}$ exp[(-57570 ± 390 cal mol^{-1})/RT] cm^3 $molecule^{-1}$ s^{-1} (10)

over the temperature range 1195 ≤ T ≤ 2494 K, where uncertainties are given at the lα level.

The mean deviation of the composite data set from the Arrhenius expression in (equ 10) is ± 26% at the lα level.

6 RECOMMENDATIONS

This work therefore suggests that further work will be required to establish accurate rate constants and the branching fraction for the reaction of O (^3P) with N_2O. Also, a study of this type requires more complex kinetic modeling to extract proper values for K_1 (T) and the overall stochiometry for the reaction considered. Upper limit values for K_2 could be estimated by carrying out more seven experimental runs if there will be support financially from some chemical sciences division in Nigeria and oversea.

References

Alley, M.T., Yetter, R.A. & Dryer, F.L (1995) International journal of Chem. Kinet Pg. 27, 883.

Baulch, D. L. Drysdale, D.D., & Lloyd, A.C (1973). Evaluated Kinetic Data for High Temperature Reactions: Butterworths: London, P. 2.

Chang, A. H. H & Yarkoney, D. R (1993) journal of Chemical Physical Sciences. Pg. 99 6824.

Dean, A. M. (1976) Int. J. Chem Kinet. 1976, 8, 459.

Dean, A.M. & Steiner, D.C. (1977) Journal Chem. Physical Science Pg. 66 598.

Ekwonu, A.M. & Egolum, E.O. (2017). A study of the Adsorptive and Oxidative Bleadching of palm oil using clay and potassium Tetraoxomanganate VII materials International journal of Chemistry, published by Canadian Centre of Science and Education. Vol. 9, No. 2 ISSN 1916 – 9698, E – ISSN 1916 – 9701.

HO, Y.S., Mackay, G. (1998). The Kinetics of sorption of basic dyes from aqueous solution by sphagnum moss peat, Canadian journal of Chem. Eng. 76 822 -827.

Johnson, J.E., Glarborg, P. & Dam-Johnasen, K. (1992) proceedings of the 24th International symposium on combustion. The combustion institute P. 917.

Klemn, R.B., Sutherland, J.W, Wickramatchi M. A. & Yarwood, G.L. (1990) journal, of Physical Science, Chem. Pg. 94 3354.

Mallard, W.G; Westley, F.; Herron, J.T. & Hampson, R.F. (1994) NIST Chemical Kinetics Database version 6.01, NIST standard Reference Database 17, & Gaithersberg.

Michael, J.V; Sutherland, J.W.; klenum, R.B. (1995) Int. Jour. of Chemistry p. 395 – 402 and references therein.

Nayward, O.O, & Trapvell, M.B.W. (1964). An excellent summary of the present state of our Knowledge of the rates, equilibrium pressures, heats and mechanisms involved in the chemisorptions of gasses on solids. "Chemisorption", 2nd edition Bulterworth & Co.W. Loud. Odoemelam, S.A. (1998) J. Chem. Soc. Nigeria, 23, 32-34.

Nwadiogbu, J.O., P.A.C. Okoye, & V.I.E. Ajiwe J.N.S.N (2014) Hydrophobic treatment of corn-cob by acetylation. Kinetic and thermodynamic studies. J. Environ. Chem.. Eng. 2 1699 – 1705.

Ogugbuaja, V.O. (2000). Adsorption Emission spectroscopy: An instrumental methodology in Analytical chemistry. Publ. the faculty of Science University, Mariduguri, 20 – 21.

Ojo, J.O., Ipinmoroti, K.O., & Adeeyiinwo, C.E. (2007). Kinetics and Mechanisms of Venadium extraction from hydrochloric acid and solutions with tri-n-butyl phosphate. Journal of chemical society of Nigeria, 32(2), 166 – 173.

Philip, M. (2004) Advanced Chemistry' Cambridge University press. ISBN 0521 566 983 CB2 IRP, United Kingdom.

Robrig, M.; Petersen, E. L, Davidson, D.F., Hanson, R.K. (1996). International journal of Chem. Kinet Pg. 28, 599.

Ross, S., & Olivier, J.P (1964) On physical Adsorption, A clear methods, results and interpretation in the area of physical adsorption interscience publishers, Inc., New York. https://doi.org/1016/j.jece.2014.06.003.